Crossover behavior in turbulent velocity fluctuations

Jens Eggers[1] and Z. Jane Wang[2]*
[1]*Universität Gesamthochschule Essen, Fachbereich Physik, 45117 Essen, Germany*
[2]*Department of Theoretical Physics, University of Oxford, Oxford, OX1 3NP, United Kingdom*
(Received 17 January 1997; revised manuscript received 13 January 1998)

We develop a simple model of the evolution of turbulence velocity differences from inertial scales to dissipative scales by taking into account the effect of the viscosity. Our model suggests that the fluctuations of the viscous scales in turbulence result in a nontrivial crossover region in the velocity structure functions. We also discuss the importance of recognizing this crossover region when interpreting the experimental results. Assuming a finite and fixed spatial resolution, the model predicts a transition in the flatness at finite Reynolds number. We relate this observation with the reported transition by Tabeling *et al.* [Phys. Rev. E **53**, 1613 (1996)], which is analyzed in detail and compared with our model. [S1063-651X(98)12204-3]

PACS number(s): 47.27.−i, 47.80.+v

I. INTRODUCTION

In this paper we use the old idea of modeling turbulence velocity difference fluctuations by a multiplicative process, which is meant to capture the basic picture of energy cascade in turbulence. Recent studies along this line include Refs. [1–3]. However, the existing models only deal with either the inertial range or the purely dissipative range statistics. Our model fills the gap by giving a continuous evolution of velocity probability distribution functions (PDFs) from large to small scales.

The main motivation for studying the crossover behavior from the inertial range to the fully dissipative range is that we believe it is relevant to the flatness measurements of the recent experiments in shear-flow driven helium turbulence inside a closed geometry [4,5]. An important difference between the closed-geometry experiments and the open-flow experiments is that in the former case the Reynolds number can only be increased by decreasing the Kolmogorov scale. This imposes severe constraints on the spatial resolution necessary to measure velocity gradients in the closed-geometry experiments. Given the current experimental results, studying the scaling behavior in the crossover range quantitatively is worthwhile. To this end we carry out a systematic study of a multifractal model that predicts the evolution of the velocity difference PDFs from large scale to the dissipative scale and apply this model to the aforementioned experiment. Although the multifractal model is not a fundamental theory of turbulence [6], we hope some of the observed gross features provide us insight into the understanding of the transition in flatness seen in the experiment around Taylor-Reynolds number 700 [5].

Within our model, we find that the predicted flatness rapidly varies over a spatial scale between 2η and 20η. This means that measurements of the flatness are extremely sensitive to the experimental resolution, which lies in this range of scales. More interestingly, the ordering of the magnitude of the flatness as a function of Reynolds number (Re) depends on the particular scale in the crossover range. We show that at a fixed scale smaller than η the flatness increases with Re as expected, but at a fixed scale in the crossover range the flatness decreases with Re. We emphasize the important difference between the scale 1η and 10η, which is often indistinguishable in order of magnitude arguments such as those made in Ref. [7].

In the next section we briefly describe the multifractal model of turbulence, and in Sec. III we generalize this idea to include viscous effects. The resulting model for PDFs is the central starting point of the paper. In Sec. IV we determine the adjustable parameters of the model using the experimental data by Tabeling's group. In Sec. V we discuss the evolution of the PDFs as a function of the separation and compute the flatness at a fixed resolution. In the final discussion in Sec. VI we review points of agreement and the discrepancies between the experimental data and the multifractal model and relate our observation to the recently reported transition in the flatness.

II. BASIC IDEA OF MULTIPLICATIVE PROCESSES IN TURBULENCE

For the completeness of the paper, we briefly review the basic idea of multiplicative processes in turbulence. Experimental studies have shown that the turbulence velocity field in the inertial range can be described reasonably by power-law scaling

$$D_q(r) = C_q (r/L)^{q/3+\delta\zeta_q}. \tag{1}$$

This power-law range is typically short, so the exponents are better defined by the method of extended self-similarity (ESS) [8]. Information on two-point correlations of the velocity field is contained in the spectrum of exponents ζ_q [9–12]. The scaling (1) can also be naively interpreted as a consequence of an underlying multiplicative process, by which the energy is cascaded progressively from eddies of size r into eddies of size r/λ. The ratio of the velocities in successive steps is a stochastic variable s_i, whose statistics

*Present address: Courant Institute of Mathematical Sciences, New York University, 251 Mercer Street, New York, NY 10012.
Electronic address: jwang@cims.nyu.edu

are determined by its probability distribution $p_s(s_i)$. The index i denotes the ith step in the cascade from a given large scale L to r:

$$u_r = u_L \prod_{i=1}^{n} s_i . \tag{2}$$

Assuming that the s_i are identically distributed and uncorrelated, we then have for the velocity moments

$$\langle u_r^q \rangle = \langle s^q \rangle^n \langle u_L^q \rangle, \quad n = -\log_\lambda \frac{r}{L},$$

and by comparison with Eq. (1),

$$\zeta_q = \frac{q}{3} + \delta\zeta_q = -\log_\lambda \langle s^q \rangle. \tag{3}$$

Since $\zeta_3 = 1$ by the Kolmogorov structure equation, we have the constraint

$$\langle s^3 \rangle = 1/\lambda. \tag{4}$$

In the following we will be making the conventional choice $\lambda = 2$. In the context of our phenomenological description, this is of a little consequence. Using the known exponent spectrum ζ_q, information on the distribution $p_s(s)$ can be extracted through its moments. Technically it is convenient to approximate p_s by a bimodal distribution

$$p_s(s) = p\,\delta(s - s_1) + (1-p)\,\delta(s - s_2). \tag{5}$$

Recently, it was proposed based on the infinitely divisible processes that the multiplier distribution is log-Poisson [13]. One might construct the multiplier distribution by studying the ratio of the locally averaged energy dissipation similar to the method used in Ref. [14]; however, we believe that the detailed shape of multiplier distribution does not alter the key qualitative results we will obtain in the crossover range. Therefore, to avoid the unnecessary complication, we use Eq. (5) as a model distribution. Imposing Eq. (4) as a constraint, the two remaining parameters can be used to reproduce the first ten moments to within experimental error [15].

Here we base our fit on the experimental exponents by Tabeling's group [16], which were obtained by using the method of extended self-similarity. We find

$$p = 0.688, \quad s_1 = 0.699, \quad s_2 = 0.947. \tag{6}$$

The predicted scaling exponents using the above parameters are compared with the experiments in Table I. The exponents agree with the established values obtained in various turbulence experiments [17,18] to within the error.

Given this simple model of a multiplier distribution, the PDF $P_j(u)$ of velocity differences on level

$$j = -\log_2(r/L)$$

can be readily calculated: It is the distribution $P_0(u)$ on the outer scale, convoluted with p_s j times, giving

TABLE I. Inertial range scaling exponents ζ_q of the velocity field. Compared are the experimental measurements and our fit [Eqs. (5) and (6)].

q	Expt.	Model
2	0.70	0.70
3	1.00	1.00
4	1.26	1.26
5	1.50	1.50
6	1.71	1.71
7	1.90	1.89
8	2.08	2.05
9	2.19	2.19
10	2.30	2.31

$$P_j(u) = \sum_{\kappa=0}^{j} \binom{j}{\kappa} \left(\frac{p_1}{s_1}\right)^{j-\kappa} \left(\frac{p_2}{s_2}\right)^{\kappa} P_0\left(\frac{u}{s_1^{j-\kappa} s_2^{\kappa}}\right). \tag{7}$$

An expression equivalent to Eq. (7), but using the random β model, was already given in [1]. Since r is a continuous variable, it is useful to generalize Eq. (7) to continuous values of j. This can be done using the Euler-McLaurin sum formula, which gives to lowest order

$$P_j(u) = \int_{\kappa}^{j} \binom{j}{\kappa} \left(\frac{p_1}{s_1}\right)^{j-\kappa} \left(\frac{p_2}{s_2}\right)^{\kappa} P_0\left(\frac{u}{s_1^{j-\kappa} s_2^{\kappa}}\right) d\kappa + \frac{1}{2}\left[\left(\frac{p_1}{s_1}\right)^{j} P_0\left(\frac{u}{s_1^{j}}\right) + \left(\frac{p_2}{s_2}\right)^{j} P_0\left(\frac{u}{s_2^{j}}\right)\right]. \tag{8}$$

This proved to be an adequate approximation of Eq. (7) for integer values of j and smoothly interpolates in between. In the next section we follow the above basic idea to model the inertial range scaling and in addition we introduce a fluctuating cutoff to model the viscous effects.

III. MODEL FOR THE PROBABILITY DISTRIBUTIONS OF VELOCITY DIFFERENCES

Our model of PDFs of velocity differences includes three basic elements: (i) the experimentally measured PDF of velocities at a large scale P_0, (ii) the multiplier distribution p_s, and (iii) the viscous cutoff mechanism. Once they are determined, we can compute the PDF of velocities for any given scale. Among the three elements, P_0 is experimentally given and $p_s(s)$ is assumed to be of the form of Eq. (5), with three parameters given by Eq. (6). We then follow an idea that was proposed in Ref. [19] and later worked out in the context of velocity gradients by Nelkin [20] and introduce a viscous cutoff scale η_c at which the local Reynolds number is equal to a fixed value. The physical idea of this cutoff is that whenever the *local* Reynolds number of an eddy reaches a critical value Re_{cr}, it is smoothed out by viscosity and the cascade stops. Since one expects the structure of small-scale velocity fluctuations to be universal, the details of the cutoff mechanism will not depend on the specific flows and thus Re_{cr} should be universal. Furthermore, because the local Reynolds number $|u_r| r/\nu$ is a fluctuating quantity, so is η_c.

These fluctuations further modify the scaling in the dissipation range in addition to the inertial range fluctuations. We remark that in previous work on the scalings of the high-order velocity derivatives [21] it was found that the strength of the largest singularity increases with the order of derivatives. The viscous cutoff fluctuations studied assumed in this paper can be viewed as a special example of the multifractal behavior of the velocity gradients.

More specifically, we can construct the following ensemble for velocity differences u_r. For convenience, all quantities are assumed to be nondimensionalized by the large scale L and the root-mean-squared velocity fluctuations on that scale

$$U_{rms}=[\langle u_L^2\rangle]^{1/2}.$$

In computing the PDFs we treat the positive and negative velocities independently. Here we only look at positive values of u_r; the negative values are treated separately, replacing u_r by its modulus. Setting $r=2^{-n}$, each ensemble member is then constructed by the following procedure.

(i) Choose a realization of the large-scale velocity field $u_0\equiv u_L$.

(ii) Multiply u_0 by random multipliers s to obtain a realization on step j until either (a) level n is reached or (b) the condition $u_j\times 2^{-j}\geqslant R$ is no longer satisfied. The constant R is simply $R=\mathrm{Re}_{cr}/\mathrm{Re}$. This cutoff level in a particular realization will be denoted by j_c.

(iii) In case (a) $u_r=u_n$ is the desired value of u_r. If the cascade has stopped due to the action of viscosity on level $j_c<n$, the velocity difference over the distance 2^{-j_c} is u_{j_c}. Therefore, on scale r we have $u_r=u_{j_c}\times 2^{j_c-n}$.

To derive probability distributions from this procedure, it is more convenient to treat the level number as a continuous variable. Accordingly, we will assume that the velocity distributions P_j on level j have been continued to all real values j, as we did in Eq. (8).

To find an explicit expression for the probability distribution of u_r, we need to find the relation between j_c and u_r. If u_0 is already smaller than R, j_c is equal to zero and the corresponding u_r is $u_0\times 2^{-n}$. Thus $j_c=0$ for $u_r\leqslant R\times 2^{-n}$. If the cascade reaches step n, u_n must have been larger than $R\times 2^n$ and thus $j_c=n$ for $u_r\geqslant R\times 2^n$. In between, the cascade is terminated by viscosity. This means that the cutoff condition $u_{j_c}\times 2^{-j_c}=R$ must be satisfied and thus $u_r=R\times 2^{2j_c-n}$. To summarize, we have

$$j_c=\begin{cases}0 & \log_2\dfrac{u_r}{R}\leqslant -n\\[2ex] n & \log_2\dfrac{u_r}{R}\geqslant n\\[2ex] \dfrac{1}{2}\left(n+\log_2\dfrac{u_r}{R}\right) & \text{otherwise.}\end{cases}\tag{9}$$

Physically, we expect the relation between j_c and u_r to be smooth, so we will be using a smoothed version of Eq. (9), given in the Appendix, which is one to one between j_c and u_r and has the property $j_c(u_r)\to 0$ for $u_r\to 0$ and $j_c(u_r)\to n$ for $u_r\to\infty$. The smoothing introduces an additional parameter Δ [cf. Eq. (A1)], which is the number of levels over which the cascade is gradually cut off. Thus the description of the viscous range introduces two parameters: Re_{cr}, which measures the relative importance of the viscous term, and Δ, which measures the effectiveness of the viscous smoothing. In a small-scale regime of universal isotropic fluctuations, we expect both to be independent of the large-scale flow. Thus once they are adjusted, they can be applied to all other flows at different Reynolds numbers.

To compute the probability distribution P_r of u_r, we express the total probability of finding u_r between $u_r(j_c)$ and $u_r(j_c+\delta)$ through the densities P_j, namely,

$$\int_{u_r(j_c)}^{u_r(j_c+\delta)}P_r(u)du=\int_{u_{j_c}}^{\infty}P_{j_c}(u)du-\int_{u_{j_c+\delta}}^{\infty}P_{j_c+\delta}(u)du,\tag{10}$$

where u_{j_c} is the velocity on level j_c, which contributed to u_r. Hence $u_{j_c}=u_r 2^{n-j_c}$. The normalization condition (10) simply expresses the fact that contributions from levels between j_c and $j_c+\delta$ correspond to the probability of cascading down at least to level j_c, minus the probability of even making it to level $j_c+\delta$. Letting δ go to zero, we obtain

$$P_r(u_r)=\frac{\partial j_c}{\partial u_r}\left\{\frac{\partial u_{j_c}}{\partial j_c}P_{j_c}(u_{j_c})-\int_{u_{j_c}}^{\infty}\left.\frac{\partial P}{\partial j}\right|_{j=j_c}(u)du\right\},\tag{11}$$

where j_c on the right-hand side of Eq. (11) can be expressed through u_r. If r tends to zero, Eq. (11) gives the distribution of velocity gradients, for which the distribution was also derived in [1]. However, the approximation of [1] just corresponds to the first term in the curly brackets, while the second term was neglected. Note that Eq. (10) automatically ensures that P_r is normalized since

$$\int_0^{\infty}P_r(u)du=\int_0^{\infty}P_0(u)du,$$

which means that P_r inherits its normalization from the top level distribution P_0. Thus Eq. (11), together with $P_j(u)$ [cf. Eq. (8)] and $j_c(u_r)$, gives an explicit formula for $P_r(u_r)$, which we implemented numerically. This is the central result of the paper, which will be explored in the sections below. We note that the well-established Obukhov scaling relation $\mu=2-\zeta(6)$ [17,13] is a direct consequence of the present model with fluctuating cutoff [22]. Moreover, it has been noted [23] that a possible explanation of ESS would be that higher moments have smaller effective cutoffs. This is consistent with the assumption about the fluctuations in cutoff scales in our model by noting that high moments are dominated by large events.

IV. COMPARISON WITH EXPERIMENT

We apply this model to a set of experimental data measured by Tabeling *et al.* [4,5,16]. The experiment measures the longitudinal component of the turbulent velocity field inside a closed cylinder filled with helium. The viscosity is varied by a technique similar to that used in the Rayleigh-Bérnard system [24,25] to achieve a variation over three de-

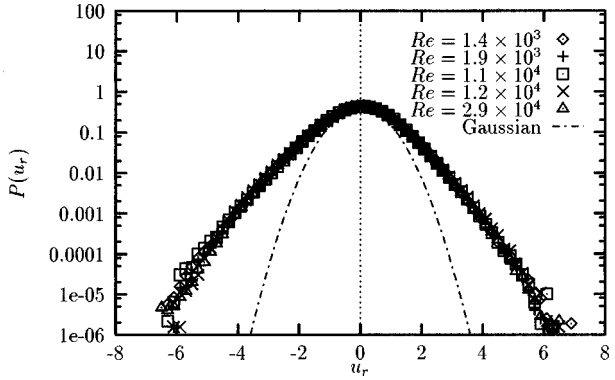

FIG. 1. PDF of the velocity difference at the outer scale L plotted on a log-linear scale for all experimental runs under consideration. The velocity differences are normalized by its variance, and the PDF is normalized to unity.

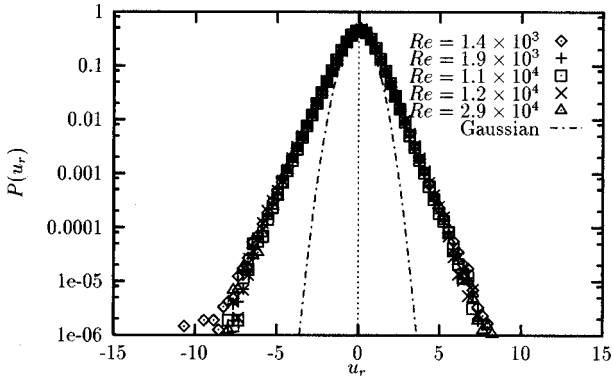

FIG. 2. PDF of the velocity difference at the scale $L/4$ (still in the inertial range) for the same experimental runs as shown in Fig. 1. Again, the velocity difference is normalized by its variance and the PDF is normalized to unity.

cades in Reynolds number. The measurements of various scaling laws are described in the above series of papers [4,5,16]. The Reynolds number dependence of the flatness is reported to have a change in character at the Taylor-Reynolds number approximately equal to 700: The flatness increases with the Reynolds number up to $\mathrm{Re}_\lambda \approx 700$ and then it decreases with the Reynolds number before increasing again. However, the origin of this transition has been subjected to much debate [26,27,7].

Because our model offers a comparison for the PDF, or equivalently for all structure functions, rather than just the scaling exponents, we can do a careful study to compare the model with the experiments and obtain a better understanding of the viscous scaling where the transition is seen. The PDF at the beginning of the cascade can be determined experimentally once we choose a sensible outer scale. Since the experiments were carried out in a fixed geometry, we expect that at a fixed outer scale, where the energy is fed in, the PDF of velocity differences is independent of the Reynolds number. We confirm this by analyzing the experimental data. By inspecting the scaling of the second-order structure functions, we choose the outer scale to be $L = 0.73$ cm for all flows. The scale is roughly 1/5 of the integral scale quoted in Ref. [4]. The reason we chose L to be somewhat smaller is that below L the scaling follows a power law and boundary effects seem to be negligible. We then examine the PDFs of the normalized velocity differences over the separation L and find that they collapse for all the flows as shown in Fig. 1. The velocities are normalized by their variance U_{rms}. In the same plot, a Gaussian distribution is shown as a dot-dashed line for comparison. The PDF at the outer scale is already non-Gaussian because we have chosen L to be smaller than the integral scale of [4], for the reasons given above. Thus some growth of intermittent fluctuations has already taken place. Also the dynamics of the boundary layer may have an important effect because the experiment is in a closed geometry. The small asymmetry of the PDF is consistent with the Kolmogorov structure equation, which gives a nonvanishing skewness of the velocity. By the construction of the model, the asymmetry will propagate down to smaller scales. The large-scale velocity variances, which differ because of different driving, set the velocity scales at each cascade level. The ratio of the velocity variance and the rotational velocity at a fixed scale will be shown later. We emphasize that the collapse of the PDFs holds for Taylor-Reynolds number (Re_λ) ranging from 300 to 2000, which includes the flows both below and above the reported transition at $\mathrm{Re}_\lambda \approx 700$. The collapse of the outer scale PDF $P_0(u)$ implies the collapse of PDF in the inertial range at a fixed separation. To check this, we calculate the experimental PDF at a separation scale of $L/4$ and again we observe the collapse of the PDFs as shown in Fig. 2.

We recall that Tabeling *et al.* observed the collapse of the PDF in the inertial range only for sufficiently large Reynolds numbers [5]. However, as we show here, the collapse works equally well for small Reynolds number ($\mathrm{Re}_\lambda < 700$ and, correspondingly, $\mathrm{Re} < 10^4$) flows in the inertial range. We suspect the reason that the previous authors did not observe the same collapse for small Reynolds number flows is because they fixed a scale too small to be in the inertial range of the small Reynolds number flows.

Because the shape of the normalized outer scale PDF is constant at the energy-input scale, the corresponding velocity scale is uniquely determined by its variance $U_{rms}(L)$. It allows us to define a Reynolds number

$$\mathrm{Re} = \frac{U_{rms}(L)L}{\nu}. \tag{12}$$

We remark that this definition is different from the one used previously [4]:

$$\mathrm{Re} = \frac{\Omega R^2}{\nu}, \tag{13}$$

where Ω is the rotation frequency and R is the radius of the apparatus. Equation (13) assumes that the velocity at the energy-input scale is proportional to ΩR. We tabulate the ratio of U_{rms} and ΩR for different Reynolds numbers in Table II and find that they vary considerably. Many factors can contribute to these differences. Apart from the systematic errors in the measurements, the shear velocity profile depends on the Reynolds number. A better understanding of the instabilities of the driving flow and the dependence of the

TABLE II. Comparison of our definition (12) of the Reynolds number and the definition (13) of the experimental group for the different flows under consideration.

Re	$\Omega R/U_{rms}(L)$
1.36×10^3	2.31
1.86×10^3	0.71
1.07×10^4	0.89
1.17×10^4	0.46
2.88×10^4	1.26

large-scale quantity $\Omega R/U_{rms}(L)$ on viscosity is desirable. For our purposes, the Reynolds number defined in Eq. (12) is adequate.

Another frequently used dimensionless quantity is the Taylor-Reynolds number

$$R_\lambda=\frac{U_{rms}\lambda}{\nu},\quad \lambda=\frac{U_{rms}}{\sqrt{(du/dx)^2}}=U_{rms}\sqrt{\frac{15\nu}{\epsilon}},\quad (14)$$

where ϵ is the average energy dissipation. The last identity assumes local isotropy of the flows. Here ϵ can be estimated by the large-scale flow

$$\epsilon=-\frac{4}{5}\frac{\langle[U(x+L)-U(x)]^3\rangle_x}{L}.\quad (15)$$

In the subsequent discussions we shall use the Re defined in Eq. (12) and the corresponding Re_λ can be found in Table III.

The remaining two parameters are Re_{cr} and Δ defined in Sec. III. The critical Reynolds number Re_{cr} defines the threshold to be compared with the local Reynolds number Re_r. If $\mathrm{Re}_r<\mathrm{Re}_{cr}$, viscous diffusion dominates and the cascade stops. In real turbulence, the termination of the cascade is a gradual process. The gradual crossover is parametrized by Δ in our model. One expects Re_{cr} and Δ to characterize the viscous cutoff mechanism, independently of large-scale flow. Ideally, one would like to choose one particular flow to fix Re_{cr} and Δ and use the same values for the rest of the flows studied. We remark that the constancy of Re_{cr} is an assumption of the multifractal theory of turbulence, which has not been checked explicitly before.

We now determine the values of Re_{cr} and Δ using the flow with $\mathrm{Re}=1.36\times10^3$. Starting from the PDF P_0 of the velocity at the outer scale, we compute the evolution of the PDFs and consequently the structure functions at smaller scales. The values of Re_{cr} and Δ are adjusted such that the resulting $D_2(r)$ agrees best with experiment. Because our algorithm allows for continuous evolution steps, we can compute a sufficient number of points along the $D_2(r)$ curve necessary for a good comparison. We find

$$\mathrm{Re}_{cr}=85\pm3,\quad \Delta=0.4\pm0.1.\quad (16)$$

TABLE III. Experimental parameters and fitted values of Re_{cr} for the experimental runs studied in this paper.

Re	$U_{rms}(L)$ (cm/s)	ν (cm^2/s)	Re_{cr}	Re_λ	η (μm)
1.360×10^3	34.93	1.88×10^{-2}	85.7	344	49.0
1.863×10^3	10.18	4.0×10^{-3}	41.0	600	20.0
1.170×10^4	18.54	1.16×10^{-3}	58.5	1626	5.9
1.073×10^4	20.52	1.4×10^{-3}	64.4	1802	6.0
2.881×10^4	44.08	1.12×10^{-3}	115.2	2394	4.1

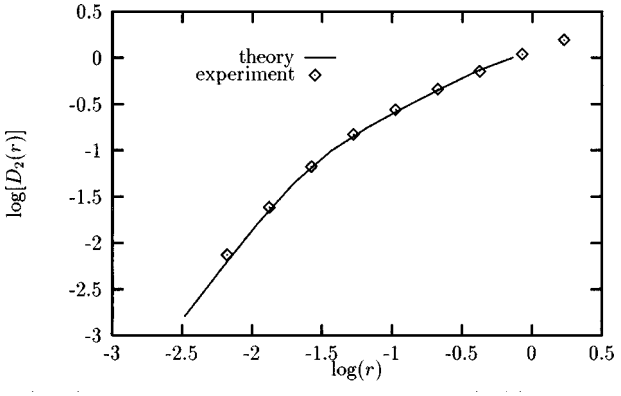

FIG. 3. log$D_2(r)$ plotted against log(r) on a log-log scale. The separation r is normalized by the outer scale L.

Figure 3 shows the comparison of the predicted $D_2(r)$ and the experimental measurement. Because the crossover in $D_2(r)$ is a sensitive function of Re_{cr}, this comparison gives a relative small fitting error, which is about 3%, as opposed to inspecting the overlap of the PDFs, which gives errors of about 15%.

We find that the predicted PDFs are insensitive to the values of Δ, which is fixed to be 0.4 for all flows. To check whether Re_{cr} is indeed independent of Reynolds number, we repeat the above procedure for all the flows. The value of Re_{cr} is shown in the fourth column of Table III. It is evident that there are considerable fluctuations in Re_{cr}, which correspond to about a factor of 2 in the value of the crossover scale between inertial and viscous range. In what follows we will use Re_{cr} as quoted in Table III for the individual runs since otherwise the fits of the PDFs in the viscous range would be poor. Unfortunately, this means that there is an adjustable parameter for each run. We will bear this in mind when we compare the theory and the experiments. From the experimental data available to us, we are not able to pinpoint the reason for the deviations of Re_{cr} from a constant value. However, these fluctuations are at least consistent with the fluctuations seen in the energy dissipation, which is about 10% [4,7].

Having determined all the adjustable parameters in the model, we can proceed to make predictions for various quantities of interest. Table III is a summary of the experimental and model parameters for the flows studied in this paper.

V. EVOLUTION OF PDFs AND THEIR ASYMPTOTICS

We start from the PDF of velocity differences at the outer scale and compute the subsequent PDFs as the scale decreases. We show the evolution of the PDFs for two typical flows: one below and one above the transition at the Reynolds number $\mathrm{Re}_\lambda\approx700$. Figure 4 shows the evolution of the PDFs for $\mathrm{Re}=1.36\times10^3$, which corresponds to the Taylor-Reynolds number $\mathrm{Re}_\lambda=344$, and Fig. 5 for $\mathrm{Re}=1.17\times10^4$ at

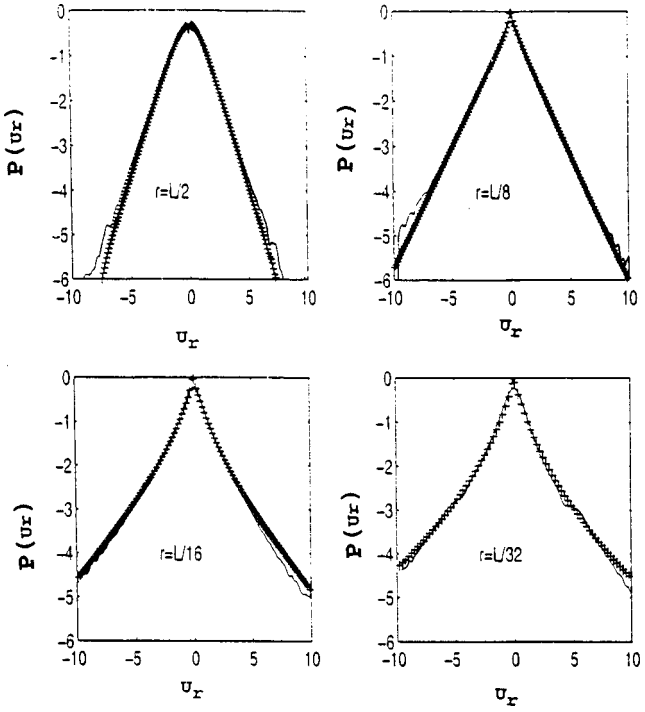

FIG. 4. Evolution of the logarithm of PDFs of velocity differences over different separations at $\mathrm{Re}=1.36\times10^3$. The velocity difference is normalized by its variance and the PDF is normalized to unity.

$\mathrm{Re}_\lambda=1626$. The solid line represents the experimental measurement, while the pluses show the theoretical prediction. Each series covers scales ranging from the outer scale to the smallest scale measured by the experiments.

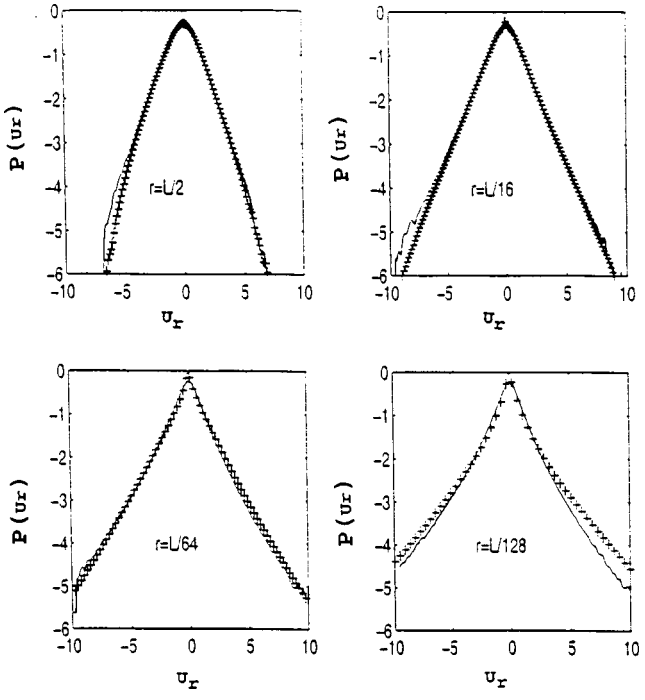

FIG. 5. Evolution of the logarithm of PDFs of velocity differences over different separations at $\mathrm{Re}=1.17\times10^4$. The velocity difference is normalized by its variance and the PDF is normalized to unity.

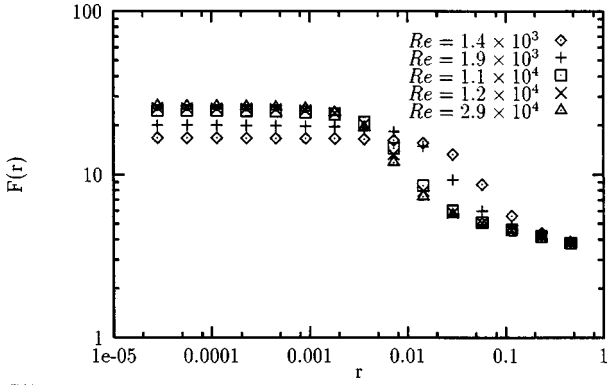

FIG. 6. Theoretical prediction for the scale-dependent flatness $F(r)$ for different experimental runs. Note the sharp rise in the crossover regime and the crossing of different curves in the same regime.

Similar pictures are obtained for all the flows we study. As expected, the shape of the PDF evolves toward stretched-exponential curves. The stretched tails describe the increasingly frequent occurrences of large intermittent events. The distribution of the large events make significant contributions to higher moments. A typical measure of intermittency is the flatness, which will be discussed below.

In the case of the smaller Re flow, theory and experiment agree down to the smallest scale resolved by the experiment. Both the experimental and the theoretical PDFs show no sign of reaching their asymptotics even at the smallest scales. In the case of the large Re flow, theory and experiment agree for a number of cascade steps, but eventually deviate as the scale decreases toward the limit of experimental resolution. While the theoretical PDF continues to evolve, the experimental PDF saturates. This saturation corresponds to a saturation in the flatness, as shown below.

We find that the theoretical PDF reaches its asymptotics only close to the Kolmogorov scale, typically at $r\sim\eta$. This then suggests that in order to understand the scaling of the velocity derivatives, the experiments need to resolve a smaller scale than they currently do, which is 9.6η for this particular flow. To see this more clearly we look at the flatness, which can be defined as the limit $r\to0$ of the ratio

$$F(r)=\frac{D_4(r)}{[D_2(r)]^2}. \tag{17}$$

Figure 6 shows the theoretical prediction for $F(r)$, where r is rescaled by L, for the Reynolds numbers studied, which is seen to saturate at a constant value F_0. This asymptotic value is consistent with a power law

$$F_0\sim\mathrm{Re}_\lambda^{0.15}. \tag{18}$$

Thus the prediction of the model agrees with that of the multifractal model and it is consistent with the recent compilation of experimental results in [27]. The most important feature we observe in Fig. 6 is the pronounced crossover behavior, which depends on the Reynolds number. In particular, although in the true asymptotic limit the flatness increases with the Reynolds number, at a fixed scale in the crossover region the flatness may decrease with Reynolds

number. Therefore, if experiments are limited to the resolution in the crossover region (which is typically $3\eta-10\eta$), it is conceivable that the experiments can yield a result that shows a decrease of flatness with Reynolds number.

One can further understand the width of the crossover range as a function of Reynolds number. The higher the viscosity, the earlier does rise of $F(r)$ set in. At the same time, the rise is sharper compared to the low-viscosity flows since the viscous cutoff fluctuates over a narrower range of scales [22]. The combined effect leads to a *reversal* in the magnitude of F at intermediate separations, the lowest Reynolds number leading to the largest value of the flatness. This suggests that one has to be extremely careful about comparing F at different Reynolds numbers if the spatial resolution is in the crossover range.

VI. DISCUSSION

We have studied in detail a model of PDFs of turbulent velocity differences with the aim of understanding the crossover below the inertial range for two reasons: (i) the crossover range is far more complex and less understood than both the inertial range and the far dissipation range and (ii) we hope to gain some quantitative understanding of the behavior of the flatness in the crossover range, which may shed some light on the recent controversy about the transition seen in the flatness [5].

In particular, we compare our model with the recent series of experiments by Tabeling's group. We find that in the small-Reynolds-number flows, the model and the experiments agree on the shape of PDFs down to the smallest scale resolved. On the other hand, in the large-Reynolds-number flows, the model shows departure from the experiment below a scale, which is on the order of 10η.

However, our model also allows us to consider the scale-dependent flatness (17). We observe that if gradients are estimated with finite spatial resolution, the flatness saturates at a given Reynolds number may even decrease, just as observed in the experiments of Tabeling *et al.* [5]. Since the completion of this work, the same group has made additional measurements of the flatness [28]. These measurements show a small rise in the flatness at higher Reynolds numbers, while confirming the transition at $\mathrm{Re}_\lambda \approx 700$. Placed within the context of all the available experimental data [27], the general trend is consistent with the power law (18) within the experimental scatter. Clearly, a rise in the flatness after an initial plateau is inconsistent with our interpretation of the transition. On the other hand, the data in [28] were taken with more than one experimental apparatus and the scatter is considerable. Therefore, it is hard to tell which of the observed trends in the closed geometry are significant. An independent confirmation of the plateau at $\mathrm{Re}_\lambda \approx 700$ within a closed geometry is clearly needed. In addition, comparisons between this model and other experiments such as large closed-geometry experiments or open-flow experiments will also be useful.

ACKNOWLEDGMENTS

We thank L. Biferale, L. Kadanoff, D. Lohse, M. Nelkin, and P. Tabeling for useful discussions. We are indebted to Tabeling's group at Ecole Normale Superieure for sharing their data with us. Z.J.W. is grateful to the hospitality of Tabeling's group during her visits that were supported by NATO Grant No. CRG-950245. She also acknowledges the support by the NSF-MRSEC Program at the University of Chicago and by the EPSRC grant through University of Oxford. J.E. was supported by the Deutsche Forschungsgemeinschaft through Sonderforschungsbereich 237.

APPENDIX: SMOOTHING

Here we briefly describe how a smooth function $j_c(u_r)$ was obtained from Eq. (9). Setting $\ell = \log_2(u_r/R)$, we first make sure that $j_c = \frac{1}{2}(n+\ell)$ smoothly merges into $j=n$ for $\ell \approx n$. A convenient parametrization is

$$\bar{j} = n + \frac{1}{2}\left[\frac{\ell - n}{2} - \left(\Delta + \frac{(\ell-n)^2}{4}\right)^{1/2}\right]. \tag{A1}$$

Here we introduced a parameter Δ, which measures the width of the transition region. In Sec. III we compare this with the viscous crossover of an experimentally measured structure function $D_2(r)$ and find $\Delta = 1$ to accurately describe experiments.

However, $\bar{j}$, as defined by Eq. (A1), still goes to $-\infty$ as $u_r \to 0$, while the lowest available level is 0. The approach of $j=0$ has to be fast enough to make $\partial j_c/\partial u_r$ go to zero as $u_r \to 0$. Namely, in view of Eq. (11) this means that

$$P_r(u_r) \approx 2^n P_0(2^n u_r), \tag{A2}$$

so one simply sees the gradient of the large-scale fluctuations, as expected. This is achieved by setting

$$j_c = \frac{1}{4}\log_2(1 + 2^{4\bar{j}}). \tag{A3}$$

We found that the details of the smoothing were inconsequential to the shape of the distribution as long as the basic properties of $j_c(u_r)$ were satisfied. Thus Eqs. (A1) and (A3) determine the function $j_c(u_r)$ that we used throughout this paper.

[1] R. Benzi *et al.*, Phys. Rev. Lett. **67**, 2295 (1991).
[2] P. Kailasnath, K. R. Sreenivasan, and G. Stolovitzky, Phys. Rev. Lett. **68**, 2766 (1992).
[3] L. Biferale, Phys. Fluids A **5**, 428 (1993).
[4] G. Zocchi, P. Tabeling, J. Maurer, and H. Willaime, Phys. Rev. E **50**, 3693 (1994).
[5] P. Tabeling, G. Zocchi, F. Belin, J. Maurer, and H. Willaime, Phys. Rev. E **53**, 1613 (1996).
[6] M. Nelkin and G. Stolovitzky, Phys. Rev. E **54**, 5100 (1996).
[7] V. Emsellem, L. P. Kadanoff, D. Lohse, P. Tabeling, and Z. J. Wang, Phys. Rev. E **55**, 2672 (1997).
[8] R. Benzi *et al.*, Phys. Rev. E **48**, R29 (1993).

[9] A. N. Kolmogorov, C. R. Dokl. Acad. Sci. URSS **30**, 301 (1941).
[10] A. N. Kolmogorov, J. Fluid Mech. **13**, 82 (1962).
[11] U. Frisch and G. Parisi, in *Turbulence and Predictability in Geophysical Fluid Dynamics and Climate Dynamics*, edited by M. Ghil, R. Benzi, and G. Parisi (North-Holland, Amsterdam, 1985), p. 84.
[12] G. Stolovitzky, K. R. Sreenivasan, and A. Juneja, Phys. Rev. E **48**, R3217 (1993).
[13] Z.-S. She and E. Leveque, Phys. Rev. Lett. **72**, 336 (1994).
[14] A. B. Chhabra and K. R. Sreenivasan, Phys. Rev. Lett. **68**, 2762 (1992).
[15] J. Eggers and S. Grossmann, Phys. Rev. A **45**, 2360 (1992).
[16] F. Belin, P. Tabeling, and H. Willaime, Physica D **93**, 52 (1996).
[17] F. Anselmet, Y. Gagne, E. J. Hopfinger, and R. A. Antonia, J. Fluid Mech. **140**, 63 (1984).
[18] B. Castaing, Y. Gagne, and E. J. Hopfinger, Physica D **46**, 177 (1990).
[19] G. Paladin and A. Vulpiani, Phys. Rev. A **35**, 1971 (1987).
[20] M. Nelkin, Phys. Rev. A **42**, 7226 (1992).
[21] K. R. Sreenivasan and C. Meneveau, Phys. Rev. A **38**, 6287 (1988).
[22] J. Eggers and S. Grossmann, Phys. Lett. **153**, 12 (1991).
[23] C. Meneveau, Phys. Rev. E **54**, 3657 (1996).
[24] D. C. Threlfall, Ph.D. thesis, University of Oxford, 1976 (unpublished); J. Fluid Mech. **67**, 1 (1975).
[25] F. Heslot, B. Castaing, and A. Libchaber, Phys. Rev. A **36**, 5870 (1987).
[26] F. Belin, J. Maurer, P. Tabeling, and H. Willaime, J. Phys. II **6**, 573 (1996).
[27] K. R. Sreenivasan and R. A. Antonia, Annu. Rev. Fluid Mech. **29**, 435 (1997).
[28] F. Belin, J. Maurer, P. Tabeling, and H. Willaime (unpublished).